Glycyrrhizin Binds to High-Mobility Group Box 1 Protein and Inhibits Its Cytokine Activities

Luca Mollica,[1] Francesco De Marchis,[2] Andrea Spitaleri,[1] Corrado Dallacosta,[1] Danilo Pennacchini,[1] Moreno Zamai,[3] Alessandra Agresti,[2] Lisa Trisciuoglio,[2] Giovanna Musco,[1,5,*] and Marco E. Bianchi[2,4,5,*]

[1] Biomolecular NMR Laboratory, Dulbecco Telethon Institute
[2] Chromatin Dynamics
[3] Dynamic Fluorescence Spectroscopy in Biomedicine
San Raffaele Scientific Institute, via Olgettina 58, 20133 Milan, Italy
[4] Faculty of Medicine, San Raffaele University, via Olgettina 58, 20133 Milan, Italy
[5] These authors contributed equally to this work.
*Correspondence: musco.giovanna@hsr.it (G.M.), bianchi.marco@hsr.it (M.E.B.)

SUMMARY

High-mobility group box 1 protein (HMGB1) is a nuclear component, but extracellularly it serves as a signaling molecule involved in acute and chronic inflammation, for example in sepsis and arthritis. The identification of HMGB1 inhibitors is therefore of significant experimental and clinical interest. We show that glycyrrhizin, a natural anti-inflammatory and antiviral triterpene in clinical use, inhibits HMGB1 chemoattractant and mitogenic activities, and has a weak inhibitory effect on its intranuclear DNA-binding function. NMR and fluorescence studies indicate that glycyrrhizin binds directly to HMGB1 (K_d ~150 μM), interacting with two shallow concave surfaces formed by the two arms of both HMG boxes. Our results explain in part the anti-inflammatory properties of glycyrrhizin, and might direct the design of new derivatives with improved HMGB1-binding properties.

INTRODUCTION

Inflammation, in the broadest sense, is a physiological, protective response to injury and infection. A complex network of cellular responses leads to the resolution of infection and/or the repair of the damaged tissue. Alterations of this process, however, are at the basis of many acute and degenerative diseases, including, among others, sepsis, atherosclerosis, and arthritis.

High-mobility group box 1 (HMGB1) protein is a nuclear protein that acts as an architectural chromatin-binding factor [1, 2]. HMGB1 was identified in 1999 as an important extracellular mediator of inflammation [3]. When cells die in a nonprogrammed way (necrosis), they release HMGB1 by simple diffusion; in contrast, cells that die in a programmed way (apoptosis) avidly retain HMGB1 bound to chromatin remnants even after eventual cell lysis

[4]. This differential behavior between necrotic and apoptotic cells makes HMGB1 the primary signal of tissue damage; extracellular HMGB1 promotes local and systemic responses in the organism, including inflammation and the activation of innate and adaptive immunity [5–7].

Activated monocytes, macrophages, neutrophils, platelets, and dendritic and NK cells can also release HMGB1 in the extracellular space [3, 8–10]. These cells do not die, but actively secrete HMGB1 in a process that is independent of the endoplasmic reticulum and the Golgi apparatus and depends on HMGB1 relocalization from the nucleus to special organelles, the secretory lysosomes [11–13].

Extracellular HMGB1 activates a large number of different physiological responses in different cell types, and can be considered a cytokine [14]. Its beneficial roles include the promotion of tissue regeneration, by attracting stem cells and inducing them to proliferate [15, 16]. However, HMGB1 plays a pathogenetic role in severe sepsis and arthritis [17, 18], and may play a role in atherosclerosis and cancer [19, 20]. Antibodies against HMGB1 can reverse sepsis caused by peritonitis in mice [21]; therefore, the identification of small-molecule inhibitors of HMGB1 might have significant therapeutic importance.

A large number of anti-inflammatory drugs exist, and the mode of action of several of these is unknown. As HMGB1 was recognized as an important proinflammatory molecule only fairly recently, it looked likely that one or more of the clinically effective anti-inflammatory drugs could exert their action by interfering with this relatively unexplored inflammatory axis. Our attention focused on glycyrrhizin, a glycoconjugated triterpene (Figure 1A) produced by the licorice plant, *Glycyrrhiza glabra*. In Japan, glycyrrhizin is administered at high doses (up to 140 mg/day) to patients with hepatitis B and C [22]. Remarkably, our own work has highlighted a possible role of HMGB1 in the pathogenesis of hepatitis [23]. The convergence of these pieces of information identified glycyrrhizin as a candidate inhibitor of the HMGB1-dependent inflammatory axis.

We show here that indeed glycyrrhizin inhibits the chemoattractant and mitogenic activities of HMGB1.
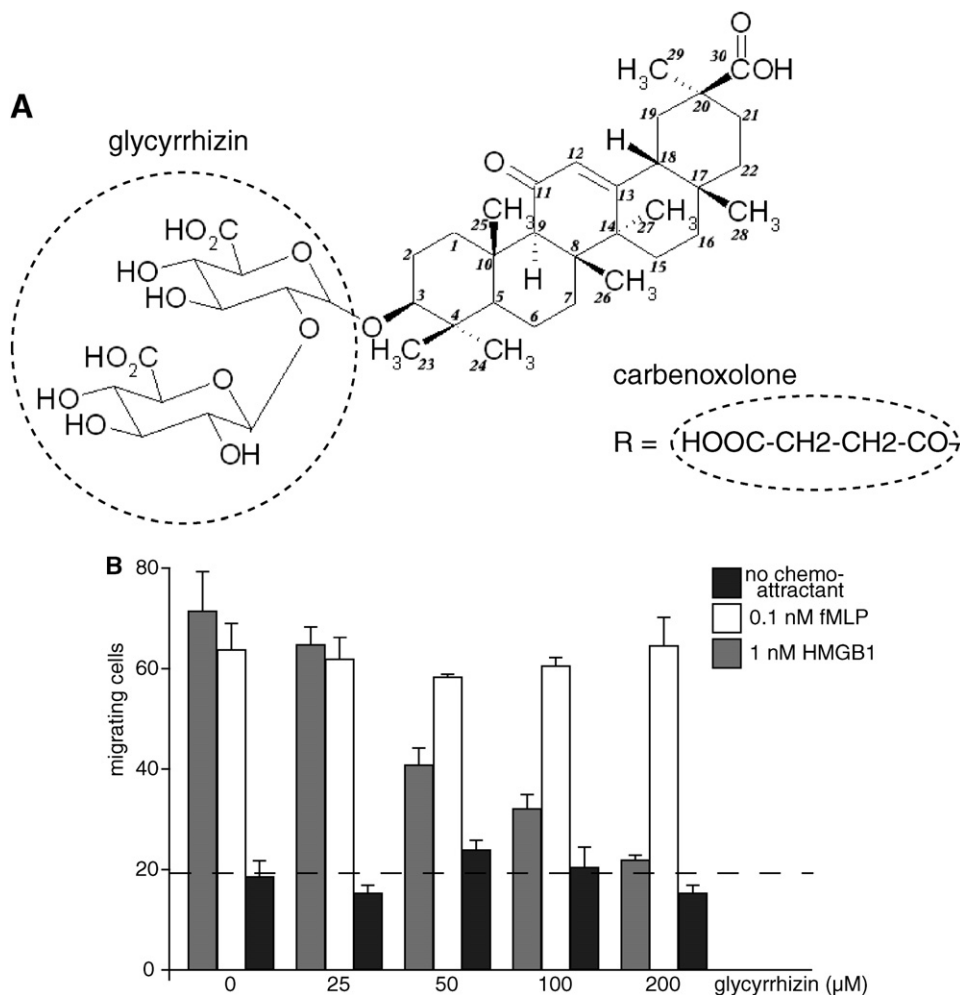
Figure 1. Glycyrrhizin Inhibits the Chemotactic Activity of HMGB1

(A) The chemical structure of glycyrrhizin. Carbenoxolone is a derivative where the two glucuronic acid residues are substituted by a succinyl residue.
(B) 3T3 fibroblasts were subjected to chemotaxis assays in Boyden chambers where 0.1 nM fMLP, 1 nM HMGB1, or no chemoattractant was added in the lower chamber, together with the indicated concentrations of glycyrrhizin. The data represent the average ± SD of three replicates; the experiments were replicated at least three times. The inhibitory effects of glycyrrhizin on HMGB1-induced cell migration were highly significant ($p < 0.001$ in ANOVA analysis), whereas they were not statistically significant on fMLP-induced cell migration.

Glycyrrhizin binds directly to each of the two HMG boxes of HMGB1, as shown by NMR and fluorescence studies.

RESULTS

Glycyrrhizin Inhibits the Chemoattractant Activity of HMGB1

HMGB1 has chemoattractant activity on endothelial, smooth muscle, and vessel-associated stem cells [15, 24]. In addition, we found that it is also a powerful chemoattractant for the widely available mouse 3T3 fibroblasts (Figure 1B). Glycyrrhizin interfered with HMGB1-elicited cell migration of 3T3 fibroblasts in a dose-dependent manner (Figure 1B; $p < 0.001$ in ANOVA two-way test). The number of 3T3 cells migrating in response to 1 nM HMGB1 was reduced by about half at a concentration of

50 μM glycyrrhizin (IC$_{50}$ = 49 ± 1 μM in a sigmoidal log dose response curve, $r^2 = 0.93$). Glycyrrhizin did not affect cell migration elicited by fMLP, a well-known chemoattractant, even at a concentration of 200 μM. This shows that glycyrrhizin does not affect the general mobility of fibroblasts, and suggests that its effect is specific on HMGB1-elicited chemotaxis. Moreover, glycyrrhizin had no statistically significant effect on the mobility of fibroblasts in the absence of chemoattractant (Figure 1B).

Glycyrrhizin Inhibits the Mitogenic Activity of HMGB1 on Vessel-Associated Stem Cells

HMGB1 promotes the in vitro proliferation of vessel-associated stem cells (mesoangioblasts) in the absence of fetal calf serum [15]. When added to mesoangioblasts in culture, increasing concentrations of glycyrrhizin
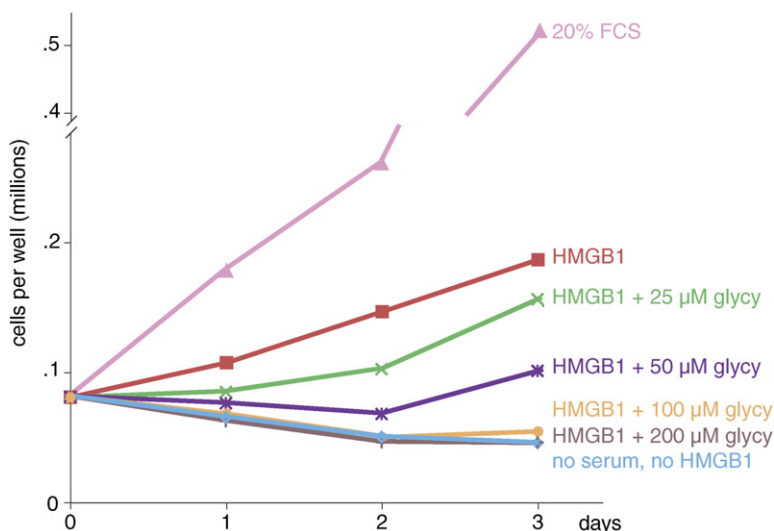
Figure 2. Glycyrrhizin Inhibits the Mitogenic Activity of HMGB1 on Vessel-Associated Stem Cells (Mesoangioblasts)

D16 mesoangioblasts were grown in RPMI medium containing no additions, 1 nM HMGB1 with the indicated concentration of glycyrrhizin, or 20% fetal calf serum (FCS). Each point represents the mean of three replicates. Error bars are omitted to avoid clutter; the standard deviation was between 2% and 15% of the average. The experiment was repeated three times. The inhibitory activity of glycyrrhizin on HMGB1-induced stem-cell proliferation is highly significant ($p < 0.001$ in ANOVA analysis).

inhibited the mitogenic activity of HMGB1 in a dose-response manner; in the presence of 200 μM glycyrrhizin no mitogenic activity of HMGB1 was noted, and the cell counts were indistinguishable from those of cultures where no serum and no HMGB1 were present (Figure 2). Conversely, glycyrrhizin showed no effect on growth of mesoangioblasts in the presence of 20% fetal calf serum (data not shown).

Glycyrrhizin Binds Directly to HMGB1: Identification of the Binding Surface by NMR

Binding of glycyrrhizin to HMGB1 was probed using NMR chemical-shift differences (CSD), a highly sensitive tool for proving interactions and for mapping binding sites and detecting residues which directly interact with the ligand or that are indirectly affected by the association. Two-dimensional ^{1}H-^{15}N HSQC spectra of full-length ^{15}N-labeled HMGB1 were recorded to monitor the changes in the ^{1}H-^{15}N chemical shifts of the backbone amide groups induced by successive additions of glycyrrhizin. A comparison of the spectra in the absence and presence of a 4-fold excess of glycyrrhizin is shown in Figure 3A. The complex is in fast exchange on the chemical-shift timescale (Figure 3B); this facilitated the assignments of the resonances in the complex, which were obtained following the crosspeaks of HMGB1 upon addition of increasing amounts of glycyrrhizin.

To identify the interaction surface, the average chemical-shift changes between the free and the bound state were plotted versus the HMGB1 residue numbers (Figure 3C). Most of the protein residues do not experience relevant chemical-shift perturbation, indicating that glycyrrhizin does not alter the overall protein structure. The global preservation of the secondary structure was further confirmed by circular dichroism (CD) spectroscopy (Figure 3F).

Resonances with significant CSD (deviating more than one standard deviation from the mean CSD) included residues F17, Q20 (side-chain protons), R23, E25, K43, and

C44 for box A (Figures 3C, 4A, and 4B) and R109, I112, D123, and A125 for box B (Figures 3C, 4C, and 4D). No interactions were observed with the linker region between the two boxes and the C terminus. The individual peaks corresponding to the acidic tail residues could not be assigned because of high spectral overlap and exchange with the solvent [25]; however, these peaks did not shift upon addition of glycyrrhizin, excluding their involvement in the binding.

Previous structural studies have clearly demonstrated that the two HMG boxes behave as rigid independent domains that do not interact with each other in the context of the full-length protein [25]; we therefore verified whether glycyrrhizin binds similarly to the two individual HMG boxes (^{15}N-labeled box A and box B) (Figures 3D and 3E). Indeed, residues mostly affected by the presence of the ligand all clustered on the first two helices of both HMG boxes, and coincided with the residues showing high CSD in the full-length protein. Additional residues located on helices 1 and 2 (H26, K42, E107, K113, G122, G129, M133) were more affected in the isolated domains than within the entire protein. This effect might be due to a slightly different orientation of the ligand, or to small structural differences of the entire protein when compared to the isolated domains.

On both HMG boxes (whether in HMGB1 or in isolation), the binding site is located at the crux of the typical L-shape fold, which has a small solvent-exposed hydrophobic surface suitable for favorable van der Waals interactions with the triterpene scaffold of glycyrrhizin (Figure 4). Interestingly, in the upfield region of the monodimensional proton spectrum of both HMGB1 and box A, variations in chemical shifts are also observed for the well-resolved ^{1}H methyl resonances of V19 and V35, located on helices 1 and 2 of box A, further suggesting an involvement of this region in the binding (see Figure S1 in the Supplemental Data available with this article online). The titration experiments also indicate that helix 3 is not involved in the binding (Figures 3C–3E and 4).
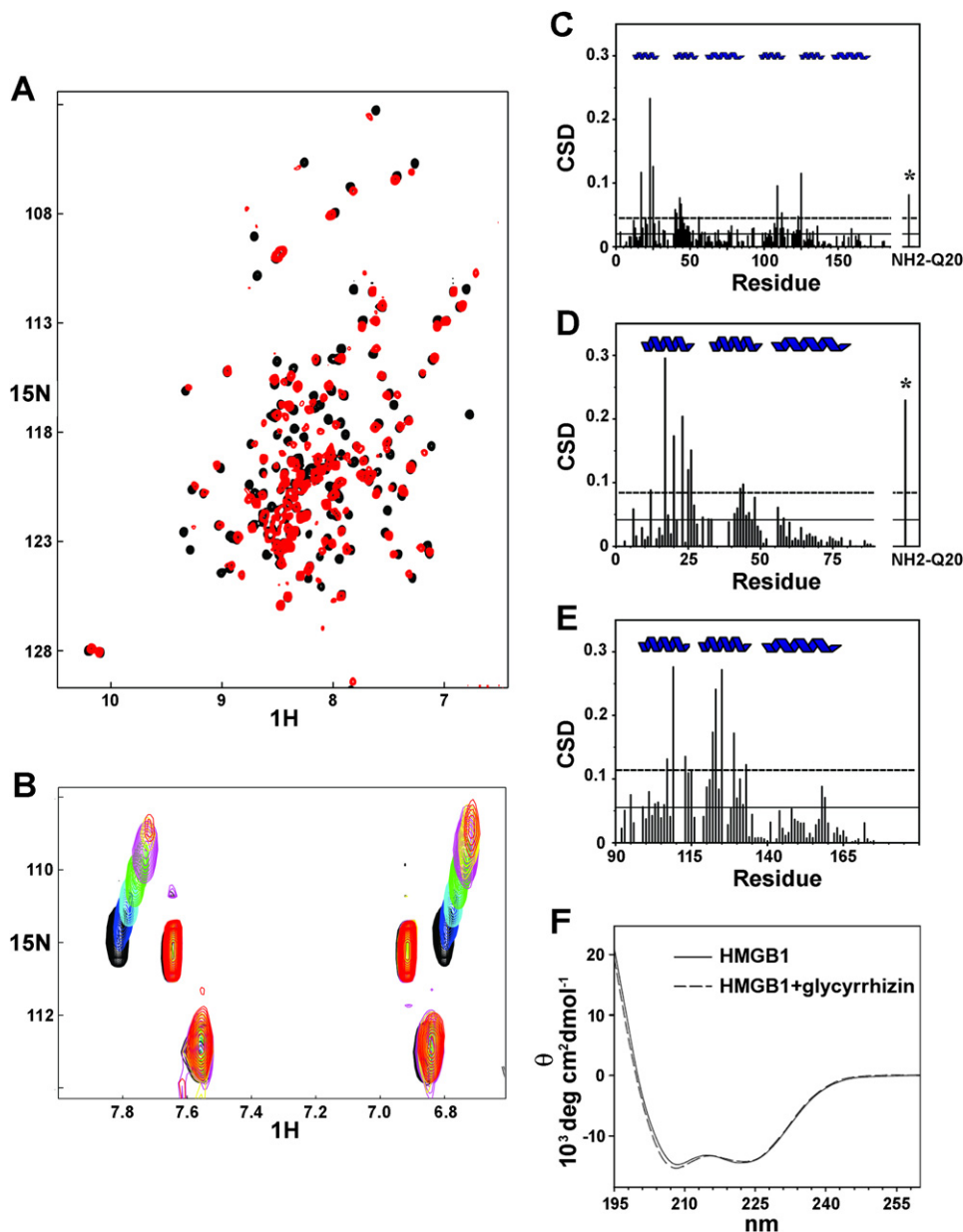
Figure 3. NMR Titration of HMGB1, Box A, and Box B with Glycyrrhizin

(A) Superposition of the HSQC spectra of HMGB1 without (black) and with (red) a 4-fold excess of glycyrrhizin. The spectra were acquired at 600 MHz, T = 298K. Protein concentration was 0.25 mM, in 20 mM phosphate buffer (pH 7.3), 150 mM NaCl, 5 mM DTT.

(B) A selected region of HMGB1 spectra during the titration with glycyrrhizin (0.5, 1, 1.5, 2, 3, 4 equivalents of ligand). The starting and end points of the titration are represented in black and red, respectively. The largest shifts were observed for the amino group of Q20. The observed chemical-shift changes are a continuous and monotonic function of the amount of added peptide, indicating that the binding is in the fast exchange limit on the NMR timescale.

(C–E) Histograms showing the value of the CSD in HMGB1 (C), box A (D), and box B (E) induced upon binding with glycyrrhizin (4-fold excess). Residue numbers are indicated on the x axis (residues for which CSD is missing are either prolines or could not be detected because of exchange with the solvent at pH 7.3); the asterisks indicate the CSD of the amino group of Q20. The continuous line represents the average chemical-shift difference; the dotted line represents the average chemical-shift difference plus one standard deviation. The amino acids mostly affected by the addition of glycyrrhizin are located on the first two helices of box A and box B (helices are schematically represented at the top of the histograms).

(F) CD spectra of HMGB1 (3 μM) without (continuous line) and with (dotted line) 200 μM glycyrrhizin. The spectra show that upon addition of an excess of ligand, the secondary structure of the protein does not change. Spectra were acquired at 20°C in 10 mM phosphate buffer (pH 7.3), 10 mM NaCl.
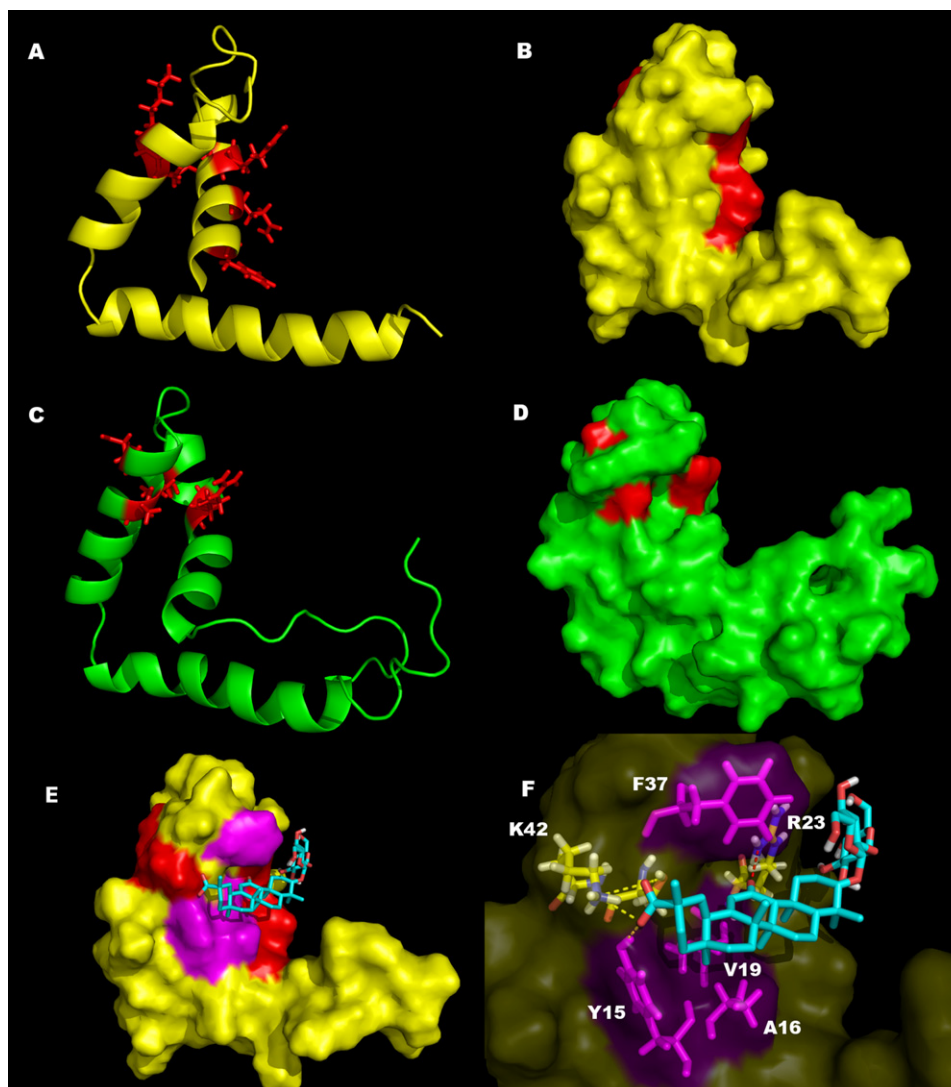
Figure 4. Mapping of the Glycyrrhizin Binding Sites and Model of Interaction

(A) Ribbon and (B) surface representation of box A (PDB code: 1aab); the side chains of residues in the full-length protein showing CSD larger than the mean value plus one standard deviation (F17, Q20, R23, E25, K43, C44) are shown in red.

(C) Ribbon and (D) surface representation of box B (PDB code: 1hmf); the side chains of residues in the full-length protein showing CSD larger than the mean value plus one standard deviation (R109, I112, D123, A125) are shown in red.

(E) Model of interaction of glycyrrhizin with box A; HADDOCK restraints and hydrophobic residues are shown in red and magenta, respectively. Glycyrrhizin (cyan) accommodates at the junction of the two arms of the L-shape fold.

(F) Zoom of the binding site: glycyrrhizin establishes favorable van der Waals interactions with the hydrophobic side chains of Y15, F37, A16, and V19 (magenta). The complex is further stabilized by a bifurcated electrostatic interaction between the carboxylate of glycyrrhizin and the amine of K42 and the hydroxyl group of Y15 (yellow dashed lines). The carbonyl group of glycyrrhizin forms a stable hydrogen bond with the guanidinium group of R23 (red dashed line).

We repeated the titrations with carbenoxolone, a derivative of glycyrrhizin where the dimer of glucuronic acid is substituted by a succinyl moiety (Figure 1A). In the case of box A, we found that the highest chemical-shift perturbations of the backbone ^{1}H and ^{15}N were again located on the first two helices, as observed for glycyrrhizin (data not shown). However, the spectra for box B and the full-length protein at higher carbenoxolone concentrations were of low quality, and showed evidence of aggregation.

Modeling of Glycyrrhizin Interaction with Box A

To further characterize the interaction between glycyrrhizin and the HMG boxes, we ran classical X-filtered experiments on the box A:glycyrrhizin complex. Because of the modest affinity of glycyrrhizin (see below), we observed very few unambiguous intermolecular interactions, which were not sufficient to calculate a structure of the complex. We therefore adopted the HADDOCK strategy [26], a recent but well-established procedure which uses

experimental chemical-shift data to drive molecular docking, both of proteins and of small molecules [27]. We obtained bundles of solutions with similar features (Figure S2), where triterpene accommodates at the junction of the two arms, establishing favorable van der Waals interactions with the hydrophobic side chains of A16, Y15, V19, and F37 (Figures 4E and 4F), whereas the sugar moieties point away from the protein. The model predicts stabilizing interactions between the carboxylate of glycyrrhizin and both the side chain of K42 and the hydroxyl group of Y15. The carbonyl group of glycyrrhizin is also predicted to create a hydrogen bond with the guanidinium group of R23 (Figure 4F).

The HADDOCK calculations suggest similar interactions between box B and glycyrrhizin: the ligand accommodates on the shallow concave surface formed by the two arms of the HMG box, creating favorable hydrophobic interactions between its triterpene scaffold and the side chains of F101, F102, I121, and A125. Similarly to box A, the model predicts electrostatic interactions of the carboxyl and carbonyl groups of the ligand with K126 and R109, respectively (Figure S3). Unfortunately, in the case of box B, we could not observe intermolecular nuclear Overhauser effects (nOes) that could further support the model.

Binding Constants for the Glycyrrhizin:HMGB1 Complex

Dissociation constants were estimated by monitoring the change of individual resonance chemical shifts of the single boxes as a function of ligand concentration. Plots of the chemical-shift changes of two representative residues for box A (R23) and box B (R109) as a function of ligand concentration are shown in Figures 5A and 5B; assuming a simple binary interaction between single boxes and glycyrrhizin, we derived K_d values of 103 ± 25 μM and 87 ± 35 μM for box A and box B, respectively. Because of the low quality of the NMR spectra of the full-length protein in the presence of glycyrrhizin at stoichiometric ratios higher than 1:4 (HMGB1:glycyrrhizin), we could not follow the NMR signals up to saturation to obtain a reliable estimate of the binding constants.

We investigated whether intrinsic fluorescence could be used to monitor the interaction of HMGB1 with glycyrrhizin. Two conserved tryptophans (W48 and W132 in box A and box B, respectively) are buried inside the hydrophobic core of the domain and do not belong to the proposed ligand binding site; as expected, no noticeable change in their fluorescence was observed (data not shown). Two tyrosines (Y15 and Y108 in box A and box B, respectively) are close to the residues showing chemical-shift perturbations; tyrosine fluorescence decreases upon glycyrrhizin addition (Figure 5C). Nonlinear least-squares fitting of the data yields dissociation constants of 170 ± 3 μM for box A and 140 ± 3 μM for box B, assuming a 1:1 stoichiometry of isolated boxes and glycyrrhizin. The binding of glycyrrhizin to both HMG boxes, together with the structural independence of the boxes inside HMGB1, strongly suggest that the full-length protein has two independent
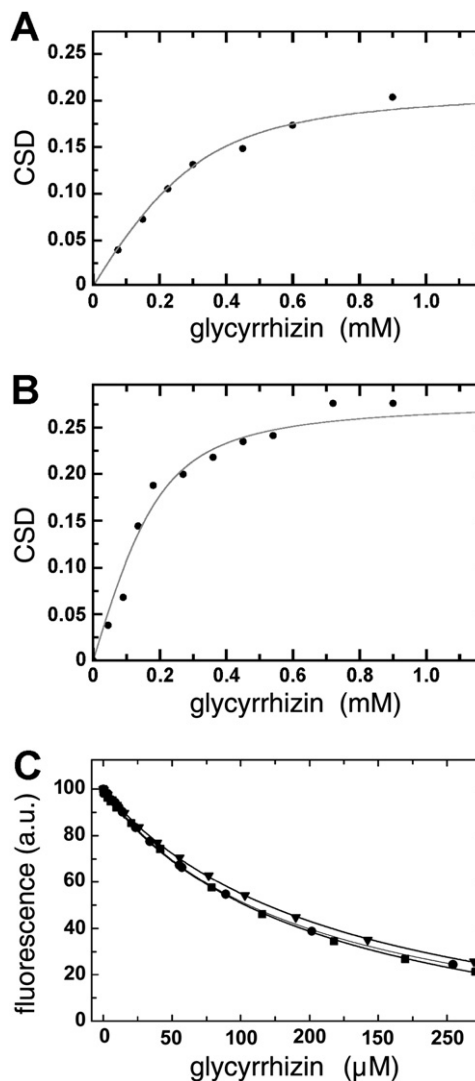

Figure 5. Glycyrrhizin Binding Isotherms to Box A, Box B, and HMGB1

(A and B) Weighted average of the R23 (A) and R109 (B) amide ^{1}H and ^{15}N chemical-shift changes as a function of added glycyrrhizin. Assuming a simple binary interaction between single boxes and glycyrrhizin, nonlinear curve fitting yields values for K_ds of 103 ± 25 μM and 87 ± 35 μM for box A and box B, respectively.

(C) Tyrosine fluorescence (excitation 273, emission 325 nm) was measured (in arbitrary units; a.u.) upon titration of glycyrrhizin into solutions of box A (triangles), box B (circles), and HMGB1 (squares). Symbols correspond to experimental data, whereas continuous curves are derived according to Equations 2 and 3 described in Experimental Procedures. Calculated dissociation constants are 170 ± 3 μM for box A and 140 ± 3 μM for box B, assuming a 1:1 association of isolated boxes and glycyrrhizin, and 156 ± 3 μM for both binding sites, assuming a 1:2 association of HMGB1 and glycyrrhizin.

binding sites for glycyrrhizin. We therefore fitted our fluorescence data for the full-length protein assuming a 1:2 (HMGB1:glycyrrhizin) binding stoichiometry and two independent dissociation constants, K_{dA} and K_{dB}, for the binding site on box A and box B, respectively. Nonlinear least-squares fitting of the data did not yield two
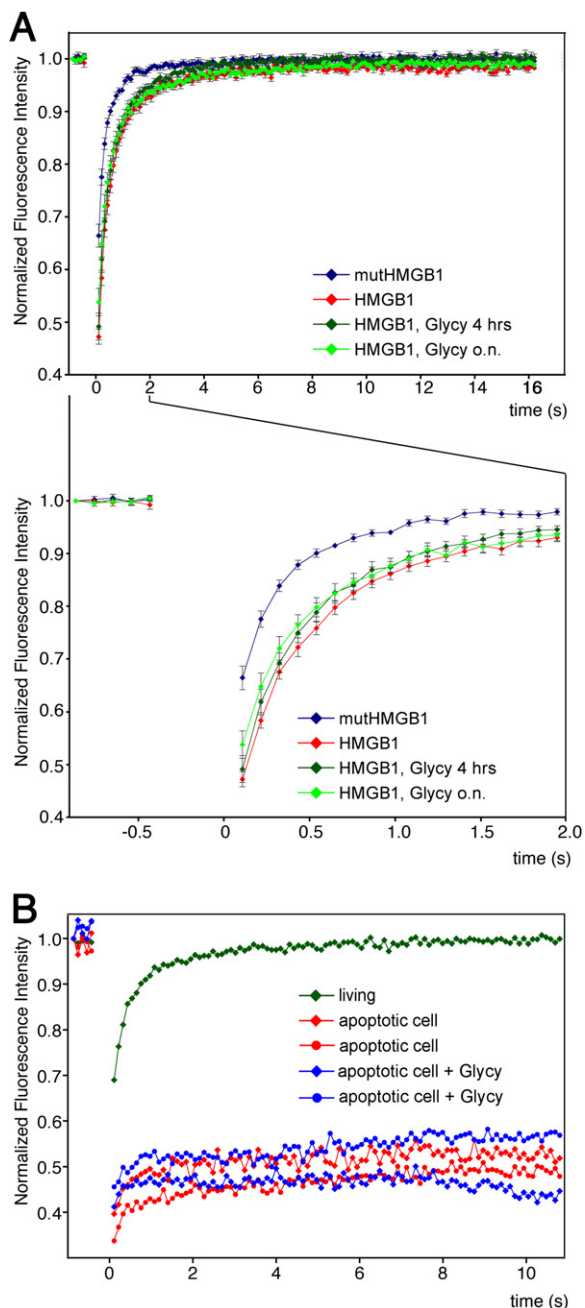
Figure 6. Glycyrrhizin Has a Limited Effect on the Intranuclear Mobility of HMGB1

(A) FRAP analysis of HMGB1-GFP in living 3T3 fibroblasts incubated in the presence or absence of 100 μM glycyrrhizin for 4 hr or overnight. Compare for reference the mobility of an HMGB1 mutant unable to bind DNA (mutHMGB1). Dots indicate mean values, and error bars indicate standard error, from eight cells. Also shown is an enlargement of the recovery kinetics in the first 2 s. The effect of glycyrrhizin is statistically significant (p < 0.01 in paired two-way t test).

(B) FRAP analysis of HMGB1-GFP in 3T3 fibroblasts undergoing apoptosis for 16 hr after addition of 2 ng/ml TNF-α and 35 μM cycloheximide in the presence or absence of 100 μM glycyrrhizin. Only two cells per class are shown out of seven analyzed, to avoid clutter. The difference between treated and untreated apoptotic cells is not statistically significant (Mann-Whitney test). For reference, the recovery kinetics of HMGB1 in living cells is indicated.

statistically different values for K_{dA} and K_{dB} but rather resulted in a common value of 156 ± 3 μM (Figure 5C). This value is similar to the value obtained for the single boxes, further suggesting that the binding of glycyrrhizin to the full-length protein is noncooperative and does not result in an improved binding affinity relative to single boxes. These results suggest also that the acidic tail does not interfere in the binding of glycyrrhizin to HMGB1.

Glycyrrhizin Interferes Only Mildly with the Intranuclear Association of HMGB1 with DNA

Interestingly, our proposed glycyrrhizin binding site on box A partially overlaps with the DNA binding site, as deduced from the crystal structure of box A complexed to cisplatin-modified DNA [28], and from other HMG box-DNA structures [29]. This raised the possibility that glycyrrhizin might interfere with the DNA-binding function of HMGB1. We then tested by fluorescence recovery after photobleaching (FRAP) whether glycyrrhizin would increase the mobility of intranuclear HMGB1, and reduce its residence time on chromatin (Figure 6A). In the presence of 100 μM glycyrrhizin, the mobility of HMGB1-green fluorescent protein (GFP) increased a little after 4 hr (p < 0.01, ANOVA), and slightly more after overnight incubation, indicating that glycyrrhizin can indeed interfere with the binding of HMGB1 to DNA in living cells. However, the glycyrrhizin-induced increase in the mobility of intranuclear HMGB1-GFP was quantitatively modest, and far from the mobility of an HMGB1-GFP mutant that does not bind DNA [30]. This suggests that the effect of glycyrrhizin on the intranuclear functions of HMGB1 is modest.

We also tested whether glycyrrhizin might interfere with the tight binding of HMGB1 to apoptotic chromatin [4]. Fibroblasts were induced to undergo apoptosis after exposure to TNF-α, in the presence or absence of 100 μM glycyrrhizin, and the mobility of HMGB1-GFP was measured by FRAP. HMGB1-GFP was immobilized both in cells treated and not treated with glycyrrhizin (Figure 6B).

DISCUSSION

We have shown that glycyrrhizin, a natural triterpene glycoconjugate derived from the root of licorice (*Glycyrrhiza glabra*), inihibits the chemotactic and mitogenic functions of HMGB1. Both NMR and fluorescence studies indicate that glycyrrhizin binds to both HMG boxes of HMGB1, without distorting their secondary structure in a significant way, as indicated by the absence of changes in the CD spectra. We also showed that the moiety of glycyrrhizin responsible for binding is its triterpene ring, because replacement of the glucuronic acid residues with a succinyl residue, as present in the drug carbenoxolone, does not interfere in the association to box A.

Chemical-shift perturbation experiments indicate that amino acids interacting with glycyrrhizin cluster at the junction of the two arms of the classical L-shape fold of both HMG boxes. A data-driven docking program that uses chemical-shift perturbation data, HADDOCK [26], generates a model of interaction between box A and

glycyrrhizin that supports the leading role of hydrophobic interactions in complex stabilization, and suggests the presence of favorable hydrophilic interactions between the carboxylate and carbonyl groups of glycyrrhizin and the conserved positively charged residues on both HMG boxes (R23, K42, R109, K126). The glucuronic acids do not appear to participate in the binding. This interaction pattern is reminiscent of the one described for DNA polymerase β: in this case as well, carbenoxolone binds on the surface of the protein, optimizing the interactions with the hydrophobic cleft formed by two helices [31].

Notably, the binding sites for glycyrrhizin on the HMG boxes partially overlap with the DNA binding sites, shielding residues such as R23, which is well known to be crucial for DNA binding [28]; in fact, glycyrrhizin reduces to a small extent the binding of HMGB1 to DNA in living cells, as assayed by quantitative microscopy. The modest effect of glycyrrhizin on the intranuclear function of HMGB1 is in agreement with the absence of cytotoxicity even at high glycyrrhizin concentrations and with the good pharmacological tolerability of glycyrrhizin in rodents and humans [32]. This is possibly due to the vast difference in the affinity of glycyrrhizin and distorted DNA for HMGB1 (on the order of 100 μM and 10 nM, respectively) [33]. Interestingly, glycyrrhizin does not cause the release of HMGB1 from apoptotic chromatin, implying that it will not produce paradoxical proinflammatory responses to apoptotic cells.

The chemotactic and mitogenic properties of HMGB1 depend on its interaction with the receptor of advanced glycation end products (RAGE) [15]. It is interesting to note that the RAGE binding surface on HMGB1 is represented by the stretch of basic amino acids between box B and the acidic tail [15], and does not correspond to the surfaces engaged by glycyrrhizin. Moreover, the IC_{50} for the inhibition of HMGB1-induced chemotaxis by glycyrrhizin is 50 μM for fibroblasts (Figure 1) and 15 μM for endothelial cells (F.D.M. and M.E.B., unpublished data), whereas the dissociation constant for glycyrrhizin and HMGB1 is about 150 μM (Figure 5). These results suggest that another surface molecule, possibly belonging to the integrin family as recently suggested [34], also takes part in the binding of HMGB1 to RAGE, and favors the binding of glycyrrhizin to HMGB1 on the cell surface.

Glycyrrhizin is known to interfere with 11β-hydroxysteroid dehydrogenase type 2, leading to an enhanced mineralcorticoid effect of cortisol [32]. However, we tested the effect of cortisol on cell migration induced by HMGB1 and fMLP, and found none (data not shown). This suggests that the effects on 11β-hydroxysteroid dehydrogenase type 2 and cell migration are distinct and separate.

SIGNIFICANCE

Our data identify in HMGB1 a target of glycyrrhizin, a useful and well-tolerated drug that has been used for decades in Japan to treat patients with hepatitis [35–37]. In turn, this suggests that HMGB1 is involved in the pathogenesis of hepatitis, and in fact we have recently shown that glycyrrhizin reduces liver disease in a mouse model of hepatitis B by interfering with HMGB1-induced recruitment of neutrophils and other inflammatory cells to the liver [23]. HMGB1 plays an important and partially unexplored role in a number of pathologies, including sepsis, rheumatoid arthritis, and atherosclerosis; the availability of a small-molecule inhibitor will facilitate future studies on the biology of HMGB1. The molecular model of the HMGB1-glycyrrhizin interaction may also help in designing more potent drugs with improved HMGB1-binding properties.

EXPERIMENTAL PROCEDURES

Cloning, Expression, and Purification of Proteins
Recombinant HMGB1 constructs comprising box A (residues 1–89), box B (residues 90–175), and the full-length protein were cloned in a modified pET-24d vector (Novagen, Madison, WI) expressing a protein with an N-terminal 6-His tag, removable by cleavage with TEV protease. After expression and cleavage with TEV protease, the proteins have a residual N-terminal three-residue tag (GAM). *Escherichia coli* cells were grown at 37°C until the optical density at 600 nm reached 0.8 absorbance units. Gene expression was induced by the addition of isopropyl β-D-1-thiogalactopyranoside (IPTG) to a final concentration of 1 mM. After 18 hr incubation at 25°C with shaking, cells were harvested by centrifugation. The cells were resuspended in lysis buffer (20 mM Tris-HCl [pH 8.0], 0.15 M NaCl, 10 mM imidazole, 2 mM β-mercaptoethanol, 0.2% NP40) and lysed by sonication. Cell debris was removed by centrifugation at 13,000 rpm for 30 min at 4°C in a microcentrifuge. The soluble 6-His-tagged HMGB1 protein was purified from the supernatant by affinity chromatography using Ni^{2+}-NTA agarose resin (Qiagen, Hilden, Germany). After several washing steps, protein was eluted in 20 mM Tris (pH 8.0), 0.15 M NaCl, 0.3 M imidazole, 2 mM β-mercaptoethanol. The 6-His tag was removed by overnight incubation at 25°C with TEV protease. During incubation, the sample was dialyzed against 20 mM Tris (pH 8.0), 0.15 M NaCl, 2 mM β-mercaptoethanol. The uncleaved 6-His-tagged protein and the TEV protease were then removed by repassing the sample over Ni^{2+}-NTA resin. The protein sample was further purified on a HitrapQ ion-exchange column followed by gel filtration on a Superdex-75 column (Amersham Biosciences, Milan, Italy) equilibrated in 40 mM Tris (pH 8.0), 0.2 M NaCl, 3 mM dithiothreitol (DTT). All the purified HMGB1 polypeptides were exchanged into appropriate buffers for NMR (20 mM sodium phosphate [pH 7.3], 0.15 M NaCl, 5 mM DTT, 0.02% NaN_3, 5% v/v D_2O). Uniformly ^{15}N- and ^{15}N/^{13}C-labeled proteins were prepared using M9 minimal bacterial growth media appropriately supplemented with ^{15}N-labeled ammonium chloride and ^{13}C-labeled glucose. Protein concentration was determined measuring the absorbance at 280 nm considering molar extinction coefficients of 9,186, 10,810, and 19,666 $M^{-1} cm^{-1}$ for box A, box B, and HMGB1, respectively.

Chemotaxis and Cell Proliferation Assays
Chemotaxis assays were performed as described [15], with the following differences: mouse 3T3 fibroblasts were used, filters were coated with a drop of 50 μg/ml fibronectin (Roche, Mannheim, Germany), and cell migration lasted 4 hr.

Cell proliferation assays were executed as described [15].

NMR Measurements
NMR spectra were recorded at 298K on a Bruker Avance 600 MHz spectrometer (Karlsruhe, Germany) equipped with inverse triple-resonance cryoprobe and pulsed-field gradients. Spectra were processed with NMRPipe [38] and analyzed using XEASY [39] and/or PIPP [40]. The ^{1}H,^{13}C,^{15}N assignment of the backbone resonances of box A, box B, and full-length HMGB1 were obtained as described [25] using uniformly ^{15}N,^{13}C-labeled samples. NMR assignments for HMGB1 and fragments thereof have been deposited in the BMRB data bank

Table 1. Residues Showing Strong Chemical-Shift Difference, nOe Interactions with Glycyrrhizin, and Flexible Residues

Domain	CSD	nOe	Flexible Residues
Box A	F17, Q20, R23, E25, H26,[a] K42,[a] K43[a]	Y15-H28[b]; F37-H27[b]; F37-H25[b]	M12-W48[a]
Box B	E107,[a] R109, K113,[a] G122, D123, A125, G129, N133[a]	n.d.	P97-A137[a]

n.d., not determined.
[a] These amino acids have been used as passive restraints in the HADDOCK calculation.
[b] These hydrogens belong to methyl groups in glycyrrhizin (Figure 1A).

(http://www.bmrb.wisc.edu) with accession numbers 15148 and 15149. Typical protein concentration for NMR titration experiments was 0.3 mM in 20 mM phosphate buffer (pH 7.3), 150 mM NaCl, 5 mM DTT. In order to minimize dilution and NMR signal loss, titrations were carried out by adding to the protein samples small aliquots of a concentrated (10 mM) ligand stock solution (glycyrrhizic acid mono-ammonium salt trihydrate, 98% purity [Acros Organics, Geels, Belgium], carbenoxolone disodium salt, 98% purity [Sigma, St. Louis, MO]) in 20 mM phosphate buffer, 150 mM NaCl, at pH 7.3. For each titration point (typically 0.25, 0.5, 0.75, 1, 1.5, 2, 3, 4 equivalents of ligand), a two-dimensional water-flip-back ^{15}N-edited HSQC spectrum was acquired with 512 (100) complex points, 55 ms (60 ms) acquisition times, apodized by 60 shifted squared (sine) window functions, and zero filled to 1024 (512) points for ^{1}H (and ^{15}N), respectively. Assignment of the corresponding amide groups in the complexes was made by following individual crosspeaks through the titration series. For each residue, the weighted average of the ^{1}H and ^{15}N chemical-shift difference was calculated as $CSD = [(\Delta\delta^2 HN + \Delta\delta^2 N/25)/2]^{1/2}$ [41].

Binding constants of glycyrrhizin to single boxes (box A and box B) were estimated by monitoring the variation of CSD of individual peaks (eight peaks for each box). Assuming a simple binary reaction between protein and ligand, dissociation constants were obtained from least-squares fitting of CSD as a function of total ligand concentration according to the relation (Equation 1):

$$\delta_i = \frac{b - \sqrt{b^2 - 4ac}}{2a},$$

with $a = (K_a/\delta_b)[P_t]$, $b = 1 + K_a([L_{ti}] + [P_t])$, and $c = \delta_b K_a[L_{ti}]$, where δ_i is the absolute change in chemical shift for each titration point, $[L_{ti}]$ is the total ligand concentration at each titration point, $[P_t]$ is the total protein concentration, $K_a = 1/K_d$ is the binding constant, and δ_b is the chemical shift of the resonance in the complex [42]. K_d and δ_b were used as fitting parameters using the Xmgrace program (http://plasma-gate.weizmann.ac.il/Grace/).

The proton chemical shifts of the bound glycyrrhizin were assigned by ^{15}N/^{13}C filter, ^{15}N/^{13}C-filtered TOCSY (60 ms) and ^{15}N/^{13}C filter, ^{15}N/^{13}C-filtered NOESY (120 ms) experiments. Intermolecular nOes between glycyrrhizin and box A were obtained from 2D NOESY experiments with ^{15}N/^{13}C filter in F2 (mixing time 70–120 ms) [43]; protein and ligand concentration were 0.6 mM and 0.9 mM, respectively.

Molecular Docking Calculations

Molecular docking of glycyrrhizin on HMG boxes (Protein Data Bank [PDB] codes: 1aab and 1hmf) was performed using the software HADDOCK 2.0_devel, which makes use of chemical-shift perturbation data to drive the docking while allowing various degrees of flexibility [26]. The protocol follows a three-stage docking procedure which includes (1) randomization of orientations and rigid body minimization, (2) simulated annealing in torsion angle space, and (3) refinement in Cartesian space with explicit water.

Residues showing chemical shifts larger than the average chemical-shift difference plus one standard deviation were used to define active residues according to the HADDOCK definition, and were used as

ambiguous interaction restraints (AIRs) [44] (Table 1). Residues that were close to the threshold, or with small (<50%) solvent-accessible surface areas, were not included in AIRs. Passive residues coincided with the region which was allowed to be flexible during the semiflexible simulated annealing step, as defined [26]. In the case of box A, intermolecular nOes were included as unambiguous restraints in the calculations only in the final run (Table 1).

Optimized parameters for liquid simulation (OPLS) were used for the protein (parallhdg5.3.pro and topallhdg5.3.pro). The geometric coordinates and parameters for the ligand were calculated and optimized using the PRODRG server [45].

During the rigid body docking, 1000 structures were calculated. The best 300 solutions in terms of intermolecular energies were selected for a semiflexible simulated annealing, followed by water refinement.

The analysis of the simulations was performed applying in-house python and tcl scripts. Root-mean-square deviations (rmsd) were calculated using the ProFit program (http://www.bioinf.org.uk/software/profit/). The fitting of the protein was performed on the flexible residues (Table 1) using the McLachlan algorithm [46]; the rmsd of glycyrrhizin was calculated only on the heavy atoms of the triterpene scaffold. The final rmsd matrix was then clustered using the algorithm described in Daura et al. [47], where a cluster is defined as an ensemble of at least two conformations displaying an rmsd smaller than 0.8 Å. The final structures were clustered and scored using a combination of energy terms (total energy, intermolecular van der Waals and electrostatic energies, restraint energies) (Figures S2B and S3B).

Fluorescence Measurements

Experiments were performed on a Varian Eclipse instrument (Victoria, Australia) with excitation at 273 nm (slit width 5 nm) and emission at 325 nm (slit width 5 nm). The initial protein concentration was 3 μM; after each ligand addition, the samples were left to equilibrate for 5 min. The ligand concentration at the end of the titration was 250 μM for box B and 270 μM for box A and HMGB1; the added ligand solution did not exceed 10% of the initial volume. At each data point, the protein concentration was corrected for the dilution due to ligand addition. All measurements were performed at 25°C in 20 mM phosphate buffer (pH 7.2), 150 mM NaCl.

Dissociation constants (K_d) for box A and box B were estimated considering a single-step binding process with an equimolar stoichiometry. The free ligand concentration in solution was considered approximately equal to the total concentration of added ligand. Experimental data were fitted by nonlinear regression (SigmaPlot 9.0, Systat Software, San Jose, CA) to the equation (Equation 2):

$$F = F_0 - \frac{F_0 - F_\infty}{[L_0] + K_d}[L_0],$$

where F is the fluorescence intensity measured at each titration point, $[L_0]$ is the total ligand concentration added at each point, F_0 is the initial fluorescence intensity of the unbound protein, and F_∞ corresponds to the fluorescence intensity of the bound final species.

K_d values for HMGB1 were estimated considering a mechanism in which two ligand molecules bind simultaneously and independently

to box A and box B. Experimental binding curves have been fitted through the following equation (Equation 3):

$$F = F_{0,A} - \frac{F_{0,A} - F_{\infty,A}}{[L_0] + K_{dA}}[L_0] + F_{0,B} - \frac{F_{0,B} - F_{\infty,B}}{[L_0] + K_{dB}}[L_0].$$

Notably, the calculated K_{dA} and K_{dB} were very similar; for this reason, we then used a model where $K_{dA} = K_{dB} = K_{d,app}$ and therefore

$$F = F_0 - 2\frac{(F_0 - F_\infty)[L_0]}{[L_0] + K_{d,app}}.$$

CD Spectroscopy

CD spectra were recorded at 293K on a Jasco 710 spectropolarimeter (Tokyo, Japan). Cuvettes with a 0.1 cm path length were used. Each spectrum was averaged using four accumulations collected in 0.1 nm intervals with an average time of 0.5 s. Typical protein concentration was 5 μM, in 10 mM phosphate buffer (pH 7.2), 10 mM NaCl. The same buffer was used to prepare a 10 mM stock solution of glycyrrhizin, which was subsequently added to HMGB1.

Fluorescence Recovery after Photobleaching

FRAP was executed as described [30]. Cells were induced to undergo apoptosis as described [4].

Supplemental Data

Supplemental Data include three figures and can be found with this article online at http://www.chembiol.com/cgi/content/full/14/4/431/DC1/.

REFERENCES

1. Bianchi, M.E., Beltrame, M., and Paonessa, G. (1989). Specific recognition of cruciform DNA by nuclear protein HMG1. Science *243*, 1056–1059.

2. Bianchi, M.E., and Agresti, A. (2005). HMG proteins: dynamic players in gene regulation and differentiation. Curr. Opin. Genet. Dev. *15*, 496–506.

3. Wang, H., Bloom, O., Zhang, M., Vishnubhakat, J.M., Ombrellino, M., Che, J., Frazier, A., Yang, H., Ivanova, S., Borovikova, L., et al. (1999). HMG-1 as a late mediator of endotoxin lethality in mice. Science *285*, 248–251.

4. Scaffidi, P., Misteli, T., and Bianchi, M.E. (2002). Release of chromatin protein HMGB1 by necrotic cells triggers inflammation. Nature *418*, 191–195.

5. Bianchi, M.E., and Manfredi, A. (2004). Chromatin and cell death. Biochim. Biophys. Acta *1677*, 181–186.

6. Dumitriu, I.E., Baruah, P., Manfredi, A.A., Bianchi, M.E., and Rovere-Querini, P. (2005). HMGB1: guiding immunity from within. Trends Immunol. *26*, 381–387.

7. Lotze, M.T., and Tracey, K.J. (2005). High-mobility group box 1 protein (HMGB1): nuclear weapon in the immune arsenal. Nat. Rev. Immunol. *5*, 331–342.

8. Dumitriu, I.E., Baruah, P., Valentinis, B., Voll, R.E., Herrmann, M., Nawroth, P.P., Arnold, B., Bianchi, M.E., Manfredi, A.A., and Rovere-Querini, P. (2005). Release of high mobility group box 1 by dendritic cells controls T cell activation via the receptor for advanced glycation end products. J. Immunol. *174*, 7506–7515.

9. Rouhiainen, A., Imai, S., Rauvala, H., and Parkkinen, J. (2000). Occurrence of amphoterin (HMG1) as an endogenous protein of human platelets that is exported to the cell surface upon platelet activation. Thromb. Haemost. *84*, 1087–1094.

10. Semino, C., Angelini, G., Poggi, A., and Rubartelli, A. (2005). NK/iDC interaction results in IL-18 secretion by DCs at the synaptic cleft followed by NK cell activation and release of the DC maturation factor HMGB1. Blood *106*, 609–616.

11. Gardella, S., Andrei, C., Ferrera, D., Lotti, L.V., Torrisi, M.R., Bianchi, M.E., and Rubartelli, A. (2002). The nuclear protein HMGB1 is secreted by monocytes via a non-classical, vesicle-mediated secretory pathway. EMBO Rep. *3*, 995–1001.

12. Bonaldi, T., Talamo, F., Scaffidi, P., Ferrera, D., Porto, A., Bachi, A., Rubartelli, A., Agresti, A., and Bianchi, M.E. (2003). Monocytic cells hyperacetylate chromatin protein HMGB1 to redirect it towards secretion. EMBO J. *22*, 5551–5560.

13. Youn, J.H., and Shin, J.S. (2006). Nucleocytoplasmic shuttling of HMGB1 is regulated by phosphorylation that redirects it toward secretion. J. Immunol. *177*, 7889–7897.

14. Yang, H., Wang, H., Czura, C.J., and Tracey, K.J. (2005). The cytokine activity of HMGB1. J. Leukoc. Biol. *78*, 1–8.

15. Palumbo, R., Sampaolesi, M., De Marchis, F., Tonlorenzi, R., Colombetti, S., Mondino, A., Cossu, G., and Bianchi, M.E. (2004). Extracellular HMGB1, a signal of tissue damage, induces mesoangioblast migration and proliferation. J. Cell Biol. *164*, 441–449.

16. Limana, F., Germani, A., Zacheo, A., Kajstura, J., Di Carlo, A., Borsellino, G., Leoni, O., Palumbo, R., Battistini, L., Rastaldo, R., et al. (2005). Exogenous high-mobility group box 1 protein induces myocardial regeneration after infarction via enhanced cardiac C-kit$^+$ cell proliferation and differentiation. Circ. Res. *97*, e73–e83.

17. Andersson, U., and Erlandsson-Harris, H. (2004). HMGB1 is a potent trigger of arthritis. J. Intern. Med. *255*, 344–350.

18. Wang, H., Yang, H., and Tracey, K.J. (2004). Extracellular role of HMGB1 in inflammation and sepsis. J. Intern. Med. *255*, 320–331.

19. Porto, A., Palumbo, R., Pieroni, M., Aprigliano, G., Chiesa, R., Sanvito, F., Maseri, A., and Bianchi, M.E. (2006). Smooth muscle cells in human atherosclerotic plaques secrete and proliferate in response to high mobility protein box 1. FASEB J. *20*, E1–E9.

20. Vakkila, J., and Lotze, M.T. (2004). Inflammation and necrosis promote tumour growth. Nat. Rev. Immunol. *4*, 641–648.

21. Yang, H., Ochani, M., Li, J., Qiang, X., Tanovic, M., Harris, H.E., Susarla, S.M., Ulloa, L., Wang, H., DiRaimo, R., et al. (2004). Reversing established sepsis with antagonists of endogenous high-mobility group box 1. Proc. Natl. Acad. Sci. USA *101*, 296–301.

22. Davis, E.A., and Morris, D.J. (1991). Medicinal uses of licorice through the millennia: the good and plenty of it. Mol. Cell. Endocrinol. *78*, 1–6.

23. Sitia, G., Iannacone, M., Muller, S., Bianchi, M.E., and Guidotti, L.G. (2007). Treatment with HMGB1 inhibitors diminishes

CTL-induced liver disease in HBV transgenic mice. J. Leukoc. Biol. *81*, 100–107.

24. Degryse, B., Bonaldi, T., Scaffidi, P., Muller, S., Resnati, M., Sanvito, F., Arrigoni, G., and Bianchi, M.E. (2001). The high mobility group (HMG) boxes of the nuclear protein HMG1 induce chemotaxis and cytoskeleton reorganization in rat smooth muscle cells. J. Cell Biol. *152*, 1197–1206.

25. Knapp, S., Muller, S., Digilio, G., Bonaldi, T., Bianchi, M.E., and Musco, G. (2004). The long acidic tail of high mobility group box 1 (HMGB1) protein forms an extended and flexible structure that interacts with specific residues within and between the HMG boxes. Biochemistry *43*, 11992–11997.

26. Dominguez, C., Boelens, R., and Bonvin, A.M. (2003). HADDOCK: a protein-protein docking approach based on biochemical or biophysical information. J. Am. Chem. Soc. *125*, 1731–1737.

27. Schieborr, U., Vogtherr, M., Elshorst, B., Betz, M., Grimme, S., Pescatore, B., Langer, T., Saxena, K., and Schwalbe, H. (2005). How much NMR data is required to determine a protein-ligand complex structure? ChemBioChem *6*, 1891–1898.

28. Ohndorf, U.M., Rould, M.A., He, Q., Pabo, C.O., and Lippard, S.J. (1999). Basis for recognition of cisplatin-modified DNA by high-mobility-group proteins. Nature *399*, 708–712.

29. Thomas, J.O., and Travers, A.A. (2001). HMG1 and 2, and related 'architectural' DNA-binding proteins. Trends Biochem. Sci. *26*, 167–174.

30. Agresti, A., Scaffidi, P., Riva, A., Caiolfa, V.R., and Bianchi, M.E. (2005). GR and HMGB1 interact only within chromatin and influence each other's residence time. Mol. Cell *18*, 109–121.

31. Hu, H.Y., Horton, J.K., Gryk, M.R., Prasad, R., Naron, J.M., Sun, D.A., Hecht, S.M., Wilson, S.H., and Mullen, G.P. (2004). Identification of small molecule synthetic inhibitors of DNA polymerase β by NMR chemical shift mapping. J. Biol. Chem. *279*, 39736–39744.

32. Ploeger, B., Mensinga, T., Sips, A., Seinen, W., Meulenbelt, J., and DeJongh, J. (2001). The pharmacokinetics of glycyrrhizic acid evaluated by physiologically based pharmacokinetic modeling. Drug Metab. Rev. *33*, 125–147.

33. Bianchi, M.E., Falciola, L., Ferrari, S., and Lilley, D.M.J. (1992). The DNA binding site of HMG1 protein is composed of two similar segments (HMG boxes), both of which have counterparts in other eukaryotic regulatory proteins. EMBO J. *11*, 1055–1063.

34. Chavakis, T., Bierhaus, A., Al-Fakhri, N., Schneider, D., Witte, S., Linn, T., Nagashima, M., Morser, J., Arnold, B., Preissner, K.T., and Nawroth, P.P. (2003). The pattern recognition receptor (RAGE) is a counterreceptor for leukocyte integrins: a novel pathway for inflammatory cell recruitment. J. Exp. Med. *198*, 1507–1515.

35. van Rossum, T.G., Vulto, A.G., Hop, W.C., and Schalm, S.W. (2001). Glycyrrhizin-induced reduction of ALT in European patients with chronic hepatitis C. Am. J. Gastroenterol. *96*, 2432–2437.

36. Yamamura, Y., Kotaki, H., Tanaka, N., Aikawa, T., Sawada, Y., and Iga, T. (1997). The pharmacokinetics of glycyrrhizin and its restorative effect on hepatic function in patients with chronic hepatitis and in chronically carbon-tetrachloride-intoxicated rats. Biopharm. Drug Dispos. *18*, 717–725.

37. Arase, Y., Ikeda, K., Murashima, N., Chayama, K., Tsubota, A., Koida, I., Suzuki, Y., Saitoh, S., Kobayashi, M., and Kumada, H. (1997). The long term efficacy of glycyrrhizin in chronic hepatitis C patients. Cancer *79*, 1494–1500.

38. Delaglio, F., Grzesiek, S., Vuister, G.W., Zhu, G., Pfeifer, J., and Bax, A. (1995). NMRPipe: a multidimensional spectral processing system based on UNIX pipes. J. Biomol. NMR *6*, 277–293.

39. Bartels, C.-H., Xia, T.-H., Billeter, M., Güntert, P., and Wütrich, K. (1995). The program XEASY for computer-supported NMR spectral analysis of biological macromolecules. J. Biomol. NMR *5*, 1–10.

40. Garrett, D.S., Powers, R., Gronenborn, A.M., and Clore, G.M. (1991). A common sense approach to peak picking two-, three- and four-dimensional spectra using automatic computer analysis of contour diagrams. J. Magn. Reson. *95*, 214–220.

41. Grzesiek, S., Stahl, S.J., Wingfield, P.T., and Bax, A. (1996). The CD4 determinant for downregulation by HIV-1 Nef directly binds to Nef. Mapping of the Nef binding surface by NMR. Biochemistry *35*, 10256–10261.

42. Johnson, P.E., Tomme, P., Joshi, M.D., and McIntosh, L.P. (1996). Interaction of soluble cellooligosaccharides with the N-terminal cellulose-binding domain of *Cellulomonas fimi* CenC. 2. NMR and ultraviolet absorption spectroscopy. Biochemistry *35*, 13895–13906.

43. Zwahlen, C., Legault, P., Vincent, S.J.F., Greenblatt, J., Konrat, R., and Kay, L.E. (1997). Methods for measurement of intermolecular NOEs by multinuclear NMR spectroscopy: application to a bacteriophage N-peptide/boxB RNA complex. J. Am. Chem. Soc. *119*, 6711–6721.

44. Nilges, M., and O'Donoghue, S.I. (1998). Ambiguous NOEs and automated NOE assignment. Prog. Nucleic Magn. Reson. Spectrosc. *32*, 107–139.

45. Schuettelkopf, A.W., and Van Aalten, D.M.F. (2004). PRODRG: a tool for high-throughput crystallography of protein-ligand complexes. Acta Crystallogr. D Biol. Crystallogr. *60*, 1355–1363.

46. McLachlan, A.D. (1982). Rapid comparison of protein structures. Acta Crystallogr. A *38*, 871–873.

47. Daura, X., Gademann, K., Jaun, B., Seebach, D., van Gunsteren, W.F., and Mark, A.E. (1999). Peptide folding: when simulation meets experiment. Angew. Chem. Int. Ed. *38*, 236–240.

Accession Numbers

NMR assignments for HMGB1 and fragments thereof have been deposited in the BMRB data bank (http://www.bmrb.wisc.edu) with accession numbers 15148 and 15149.